Design and Analysis of an Integrated Optical Sensor for Scanning Force Microscopies

Coskun Kocabas and Atilla Aydinli, *Member, IEEE*

***Abstract*—In this paper, a novel probe for displacement sensing will be introduced. It is based on a conventional GaAs cantilever, integrated with a Bragg grating as a photo-elastic strain sensor. The deflection of the cantilever is measured directly from the intensity modulation of the reflected light. The principle of the experimental setup and the sensor, as well as the theoretical investigation of the force and displacement sensitivity of the probe, is presented. Finite-element method simulations were performed to get the optimum sensor design. Transfer matrix method simulation of the waveguide grating have been described in detail. In order to enhance the sensitivity, different types of grating structures are discussed. Using this new design, it should be possible to achieve sensitivities, defined as the fractional change in detected optical power per unit displacement of the cantilever, as high as 10^{-4} Å^{-1} of cantilever deflection.**

***Index Terms*—Atomic force microscopy (AFM), cantilevers, optical displacement sensors, stress-optic effect.**

I. Introduction

THE advent of atomic force microscopy (AFM) [1] introduced a very powerful tool to investigate the surfaces of conducting and nonconducting materials with very high sensitivity. The implementation of AFM for surface study led to many different methods, i.e., Martin *et al.* [2] introduced the noncontact AFM technique to investigate the material parameters at nanometer scale, and Matthew *et al.* [3] presented the first study of frictional forces of surface atoms. AFM is based on sensing the forces between the tip and the surface of interest. The sensor used to measure the deflection of the cantilever is crucial in determining the performance and the sensitivity of the microscope. These displacement sensors are categorized mainly into two groups; external and integrated sensors. External sensors based on optical interferometers [4], optical levers [5], and interdigital detection [6] have been used. All these sensors make AFM oversized and complicated and also they require alignment of the laser beam and the detector during scanning, which limits the size of the sample that can be imaged. These disadvantages can be eliminated using integrated deflection sensors. This principle was successfully applied by Tortonese *et al.* [7]. Integrated sensors are mostly based on piezoelectric and piezoresistive sensing elements. Integrated sensors allow in-situ operation of AFM where external optical detection would be cumbersome, especially in UHV systems and harsh environmental conditions. It should be mentioned that in general integrated sensors have less displacement sensitivity (defined as fractional change in detected optical power per unit displacement of the cantilever is typically $\sim 10^{-7}$ Å^{-1} [9]) than external sensors (maximum sensitivity $\sim 10^{-4}$ Å^{-1} [6]). A recent exception is the single-electron transistor [8] integrated cantilever providing displacement sensitivity at the quantum limit. However, this device needs to be operated at 30 mK and 8 Tesla magnetic field. Other efforts to increase sensitivity of integrated sensors and to fabricate highly sensitive cantilevers have also been made [9], [10]. In this paper, we propose a novel highly sensitive integrated optical sensing element [11] for applications in scanning force microscopies. This new design consists of an integrated optical waveguide loaded with a Bragg grating (BG) which acts as a photoelastic strain sensor. A similar method was used for an opto-mechanical accelerometer [12]. In Fig. 1, we schematically draw the cantilever integrated with a waveguide loaded with a BG. GaAs has been chosen as the suitable material for fabricating the cantilever since GaAs exhibits strong photo-elastic effect. The deflection of the cantilever is detected by a shift in the resonant frequency of Bragg reflector. This optical sensor is characterized and the geometry of the cantilever is optimized for maximum sensitivity. In order to improve the design, we studied different types of BGs. The optimization of mechanical properties of cantilevers was carried out using finite-element method (FEM) simulations, while transfer matrix method (TMM) was employed to design BGs.

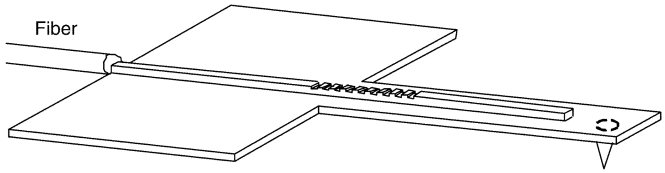

Fig. 1. BG-loaded waveguide extending across the cantilever. BG is situated at the supporting point of the cantilever.

II. Operation Principles

BGs are extensively used as wavelength selective elements in optical devices. A BG is formed by creating a periodic corrugation or refractive index modulation in optical waveguides or fibers. BGs are useful because of their frequency dependent reflection spectrum and they are, in general, characterized by a central wavelength and the bandwidth of the reflection band. These structures can be thought of as one dimensional diffraction gratings which diffract light from a forward travelling mode

Manuscript received July 23, 2003; revised January 12, 2004. This work was supported in part by the Bilkent University Research Fund (Phys-03-02) and in part by the Scientific and Technical Research Council of Turkey (TUBITAK Project No. 199E006). The associate editor coordinating the review of this paper and approving it for publication was Dr. John Vig.

The authors are with the Bilkent University, Department of Physics, 06800, Ankara, Turkey (e-mail: aydinli@fen.bilkent.edu.tr; ckocabas@fen.bilkent.edu.tr).

Digital Object Identifier 10.1109/JSEN.2005.846172

1530-437X/$20.00 © 2005 IEEE

into a backward travelling mode. From the well-known Bragg condition, the central wavelength of the grating can be written as

$$\lambda_B = m2n_{\text{eff}}\Lambda \tag{1}$$

where n_{eff} is the effective index of the structure and Λ is the period of the grating and m is an integer number. The bandwidth of BG, $\Delta\nu$, is proportional to the effective index modulation, Δn_{eff} and is approximately given by

$$\frac{\Delta\nu}{\nu} = \frac{\Delta n}{n_{\text{eff}}}. \tag{2}$$

The effect of the grating on the propagation of light can be modeled using coupled-mode theory (CMT). CMT [13] predicts that the peak reflectivity of a BG is given by

$$R_{\max} = \tanh^2(\kappa L) \tag{3}$$

where L is the grating length and κ is the grating strength (coupling coefficient). Waveguide BGs can be formed by physically corrugating the waveguide surfaces as is done in DFB lasers. Reflection spectrum of BG depends on the effective index of the waveguide, any variations of the refractive index result in the change of the reflection spectrum. Therefore, BGs have been applied to sense a number of physical values including strain [14], temperature [15] and magnetic fields [16]. These applications are based on the same principle, i.e.: measurement of Bragg wavelength shift caused by external effects. In all these methods, a broadband optical source, such as a LED or a superfluorescent device, is used as the light source. To measure the shift in wavelength, external spectrum analyzers are employed. Recently, many signal-processing methods are developed to directly measure the intensity modulation of the reflected light [17]. In one method, a light source with a very narrow spectral width such as DFB laser, is used in conjunction with a BG. Typically, a BG has much larger spectral width (0.5 nm) than a DFB laser (~ 1 pm). If the laser wavelength coincides within the reflection spectrum of BG, the reflected light associated with the laser can be detected at the output. The output intensity at the detector is proportional to the overlap integral of the function $f(\lambda - \lambda_L)$ and $g(\lambda - \lambda_g)$ representing the spectral characteristics of the laser and BG, respectively [17]. Assuming these functions as Gaussians, we can write

$$f(\lambda - \lambda_L) = P_0 \frac{2}{\Delta\lambda_L}\sqrt{\frac{ln2}{\pi}} \exp\left[-4ln2\left(\frac{\lambda - \lambda_L}{\Delta\lambda_L}\right)^2\right] \tag{4}$$

$$g(\lambda - \lambda_g) = R \exp\left[-4ln2\left(\frac{\lambda - \lambda_g}{\Delta\lambda_g}\right)^2\right] \tag{5}$$

where $\Delta\lambda_L$ and $\Delta\lambda_g$ are the spectral widths and λ_L and λ_g are the central wavelengths of laser and grating, respectively, and P_0 is the total power of the laser and R is the reflectivity of the grating. The overlap integral can be written as

$$I_{\text{out}} = \int_0^\infty f(\lambda - \lambda_l) g(\lambda - \lambda_g) d\lambda. \tag{6}$$

Since the spectral width of BG, $\Delta\lambda_g$, is much larger than that of the laser, $\Delta\lambda_L$, I_{out} is

$$I_{\text{out}} \simeq P_0 g(\lambda_L - \lambda_g) \tag{7}$$

$$I_{\text{out}} = P_0 R \exp\left[-4ln2\left(\frac{\Delta\lambda_c}{\Delta\lambda_g}\right)^2\right] \tag{8}$$

where

$$\Delta\lambda_c = \lambda_L - \lambda g. \tag{9}$$

Defining Bragg wavelength as

$$\lambda_g = 2n_{\text{ef}}\Lambda \tag{10}$$

we can write

$$I_{\text{out}} = P_0 R \exp\left[-4ln2\left(\frac{\lambda_L - 2n_{\text{ef}}\Lambda}{\Delta\lambda_g}\right)^2\right]. \tag{11}$$

From (11), it is clearly seen that output intensity depends on the effective index of the grating. Any changes in effective index of the grating due to external effects, modulates the output intensity. From this modulation, it is possible to determine the external physical quantity. The most sensitive operation can be achieved by tuning the laser wavelength such that $\Delta\lambda_c = \Delta\lambda_g/2$ where the slope of reflection onset is maximum. Among the advantages of this method are that, it does not require any spectrum analyzer or a filter, it is all optical and integrated. It should also be mentioned that I_{out} depends strongly on the reflection spectrum. Narrow bandwidth provides higher sensitivity.

III. Cantilever Design

In any cantilever design, the measurement of the displacement of the cantilever with high sensitivity is the essential task. The design of the cantilever and the type of the integrated sensor plays a fundamental role to increase the sensitivity. Previously, work have been done to enhance the sensitivity of AFM through stress engineering of the cantilever [18]. Bending of the cantilever generates stress which is the necessary physical quantity used to characterize the displacement of the cantilever. In this work, photo-elastic effect is used for the sensing mechanism; stress generated on the cantilever changes the refractive index of the waveguide where the BG is loaded. Furthermore, sensing the generated stress using integrated optical devices requires materials suitable for such devices with large stress optic coefficients. A good candidate is GaAs. Applying mechanical stress to GaAs results in variation of local index due to photo-elastic effect. Since the displacement of the tip causes mechanical stress along the cantilever, maximizing the stress on the sensing element will maximize the performance. Therefore, the sensing element is placed at the supporting point where the stress reaches its maximum value of

$$\sigma_{\max} = \frac{3Et}{2l^2} z \tag{12}$$

where E is the Young's Modulus, t is the thickness, l is the length, and z is the displacement of the cantilever. The design

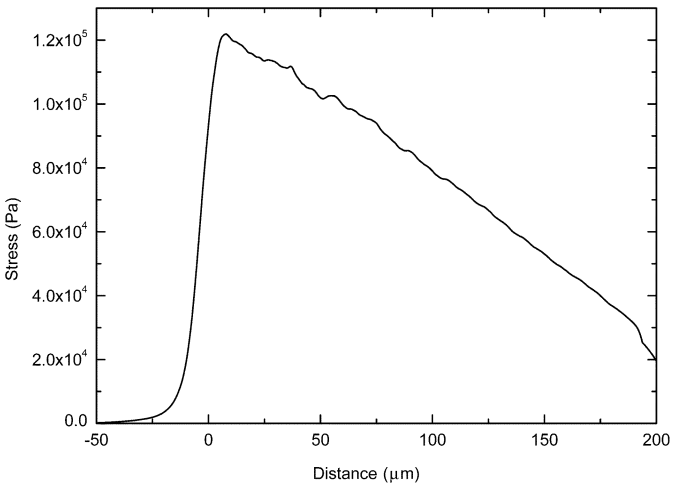

Fig. 2. Simulated stress distributions along the length of the cantilever.

of the grating, waveguide, and cantilever is related to the stress distribution on the cantilever. Fig. 2 shows the stress along the waveguide obtained from FEM simulations. For FEM simulations, Young's Modulus of 0.83×10^{11} N/m^2, and Poisson's ratio of 0.31 were used. Static stress analysis was performed using ANSYS software. The mesh was increased in the waveguide region where the grating sensor is placed. Maximum stress occurs at the supporting point of the cantilever and decreases linearly along the cantilever length. The analysis performed here uses the stress at the surface of the cantilever. Stress reaches its maximum value on the surface and decreases along the thickness of the cantilever also. The waveguide height is much smaller than the cantilever thickness; therefore, the variation of the stress along the waveguide height is neglected and an average value is used. These results are used in the design of the sensor and calculation of the sensitivity. Through the photo-elastic effect index change can be written as [13]

$$n_{\text{eff}} = n_0 + \sum_i C_i \sigma_i \tag{13}$$

where C_i is the stress-optic constant of the waveguide and σ_i is the local stress. For GaAs, longitudinal stress-optic coefficient $C_l = 1.7 \times 10^{-11}$ Pa^{-1} and transverse stress-optic coefficient $C_t = 1.0 \times 10^{-11}$ Pa^{-1}. Longitudinal stress on the cantilever surface is much larger than the transverse stress; therefore, we can neglect the transverse stress and obtain

$$\Delta n \simeq C_t \sigma_l \simeq \frac{3C_t E t}{2l^2} z \tag{14}$$

and the effective index becomes

$$n_{\text{eff}} = n_0 + \frac{3C_t E t}{2l^2} z. \tag{15}$$

Putting this equation into (5), the output intensity as function of cantilever displacement is obtained as

$$I_{\text{out}} = P_0 R \exp\left[-4ln2\left(\frac{\lambda_L - 2\Lambda\left(n_0 + \frac{3C_t E t}{2l^2} z\right)}{\Delta\lambda_g}\right)^2\right]. \tag{16}$$

In a more rigorous treatment, it would be necessary to include the stress contribution as a function of cantilever length, which will give a chirped response instead of a Gaussian. However, as can be seen from Fig. 2, the index change is linear and for the sake of simplicity, we assume an average value for the refractive index change and neglect second order effects. Since final calculations are done numerically using TMM, where stress contributions to refractive index are included and is seen to agree reasonably with the simplified Gaussian approach, we take this approximation as valid for our parameter range.

From Hooke's law, force on the tip of the cantilever can be expressed as

$$F = kz = \frac{wEt^3}{4l^3} z \tag{17}$$

where k denotes the spring constant of the cantilever. Using (17), (16) can also be written as a function of force applied on the tip

$$I_{\text{out}} = P_0 R \exp\left[-4ln2\left(\frac{\lambda_L - 2\Lambda\left(n_0 + \frac{6C_t l}{wt^2} F\right)}{\Delta\lambda_g}\right)^2\right]. \tag{18}$$

Equations (16) and (18) show that by measuring the output intensity, it is possible to calculate the displacement of the cantilever and the force applied on it. It can be seen that the local index variation, and, therefore, the output intensity is strongly dependent on the geometry of the cantilever and the reflection spectrum of the BG.

IV. Bragg Grating Design

Waveguide BG is designed to be fabricated on a single-mode *GaAs/GaAlAs* waveguide. The operational parameters for the BG are the period and the grating height of the grating. The central wavelength can be controlled by tuning the period and the coupling coefficient can be controlled by tuning the grating height. Fig. 3 shows the calculated TE mode profile for a *GaAs/GaAlAs* ridge waveguide. By choosing the Al concentration at %20, it is possible to have an index contrast of 0.12 and choosing the core height as 1 μm and ridge width as 2 μm, a single-mode waveguide can be obtained. The mode spectrum of such a waveguide was calculated using beam propagation method (BPM) simulation to confirm the single-mode behavior. The analysis of the grating has been carried out by calculating the coupling coefficient, κ. Using CMT, κ can be written as [19]

$$\kappa = \frac{{k_0}^2}{2\beta N^2} \int_{\text{corrugate}} \Delta[n^2(x,z)] E^2 dx \tag{19}$$

where $k_0 = (2\pi/\lambda_0)$ and β is the propagation constant, E^2 is the electric field profile and N^2 is the normalization constant given as

$$N^2 = \int_{-\infty}^{\infty} E^2 dx. \tag{20}$$

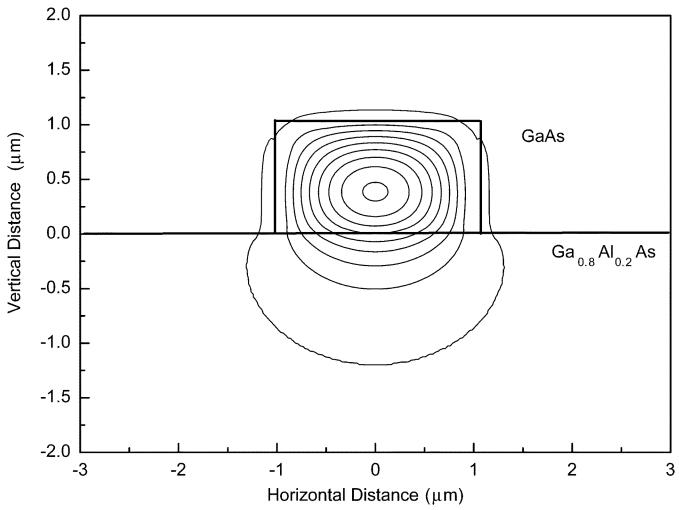

Fig. 3. Calculated TE profile of a single-mode GaAs/GaAlAs rib waveguide.

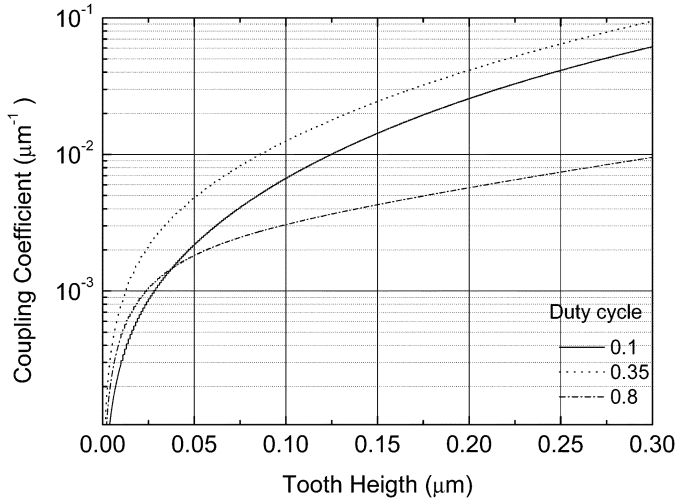

Fig. 4. Coupling coefficient as a function of tooth height for three different duty cycles.

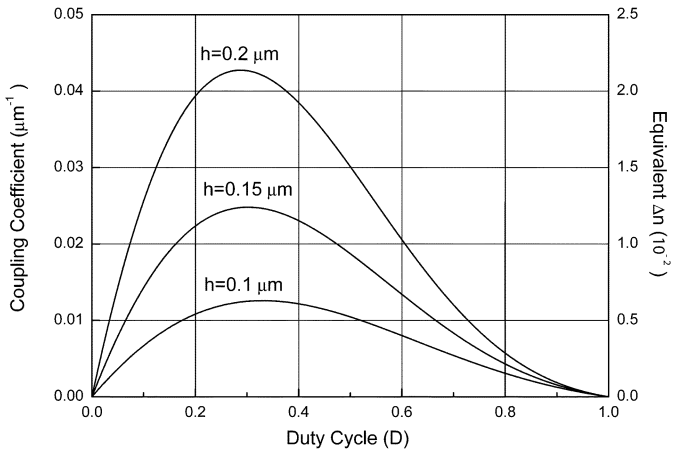

Fig. 5. Coupling coefficient and equivalent index change as a function of duty cycle.

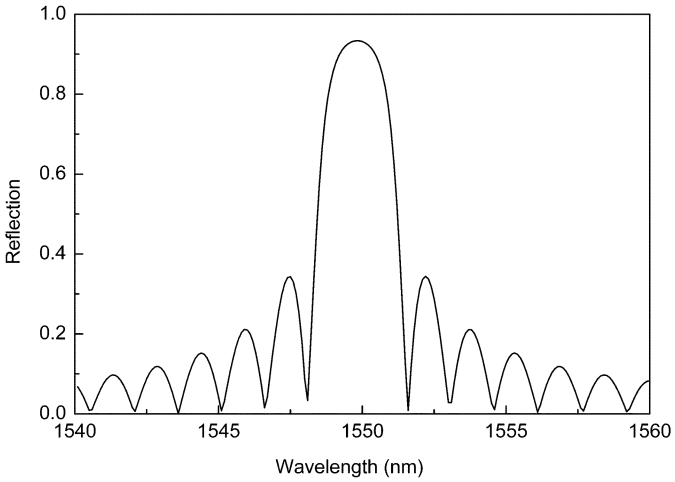

Fig. 6. Reflection spectrum of the BG used to sense tip displacement.

Fig. 4 shows the calculated coupling coefficient for this waveguide as a function of grating height (tooth height) for three different duty cycles. Coupling coefficient κ increases rapidly as the tooth height increases. For a first order diffraction grating with grating height of $h = 0.1$ μm, the coupling coefficient is seen to be $\kappa = 0.01$ μm^{-1}, for a duty cycle of 0.35. This grating depth is chosen so as to minimize the optical loss. In order to make the reflectivity R larger than 0.9, it must be such that $\kappa L \geq 2.18$. Therefore, minimum grating length must be $L \geq 200$ μm which is suitable for cantilever design. It should be noted that there is a tradeoff between L and κ due to the fact that to get higher reflectivity κ must be increased, which causes the broadening of the spectral response leading to a decrease in sensitivity. Duty cycle of a grating is defined as the ratio of grating tooth to grating period. In Fig. 5, we plot the coupling coefficient as a function of duty cycle for various grating depths. One interesting result which is observed from Fig. 5 is that the strongest coupling occurs when the duty cycle is smaller than 0.5. In our design, a duty cycle of 0.35 was chosen to obtain the largest coupling coefficient with the smallest loss. Fig. 6 shows the calculated reflection spectrum of the BG about the central wavelength of 1.55 μm. This spectrum is calculated using TMM simulation. In the simulation, we use the effective index change (δn) calculated from the coupling coefficient such as

$$\delta n = \frac{\kappa \lambda}{\pi} \tag{21}$$

which shows good agreement with that obtained from CMT. In the numerical implementation of TMM, we model the BG using parallel layers, where stress contribution to refractive index is included using the numerical results of the stress simulations.

In order to get high sensitivity, a BG with a high reflectivity and narrow spectral width is used. Using grating period of 210 nm and a total height of 0.1 μm, a BG with 0.9 reflectivity and 3-nm reflection bandwidth was obtained. Increasing the number of periods in the BG narrows down the stopband. However, for typical cantilever lengths, the number of periods to be used in the construction of a BG is limited. Increasing the coupling coefficient κ by choosing large tooth heights would also yield a higher reflection; however, large tooth heights may lead to unacceptable optical looses which should be avoided. As the operational point of the sensor is to be chosen at the

TABLE I
COMPARISON OF HIGH AND LOW STIFFNESS CANTILEVERS

$w(\mu m)$	$t(\mu m)$	$L_c(\mu m)$	$L_g(\mu m)$	$f_0(\ kHz)$	$k(\ N/m)$	$S_d(\mathring{A}^{-1})$
50	5	200	100	50	16	$1.0\ 10^{-4}$
50	5	1000	500	2	0.1	$1.1\ 10^{-7}$

maximum slope, operation of the sensor is not affected directly by the side lobes.

In Table I, we summarize the width ω, and length L_c of the cantilever, the calculated sensitivities S_d, spring constants k, and resonant frequencies f_0, both of a high stiffness and a low stiffness cantilever with identical BGs of two different lengths L_g. Grating period and tooth height were taken as 210 and 100 nm, respectively. From Table I, it is clear that in the noncontact mode, the high stiffness cantilever exhibits higher displacement sensitivity than low stiffness cantilever, as expected. The Young's Modulus of 0.83×10^{11} N/m^2, Poisson's ratio of 0.31, longitudinal stress-optic coefficient of $C_l = 1.7 \times 10^{-11}$ Pa^{-1} were used for GaAs cantilevers in these calculations. In Section V, further improvement of these parameters is presented.

V. QUARTER-WAVE SHIFTED BRAGG GRATING

The sensitivity of a BG sensor strongly depends on the reflectivity spectrum, and, hence, the bandwidth of the sensor. A further improvement of the design can be made using narrowband, highly reflective filters. One way to implement a narrowband filter is to use a quarter-wave shifted BG (QWBG). Haus [20] showed that insertion of a quarter wave shift at the center of BG provides a single narrow bandpass filter in the stopband of the BG. The transmission spectrum of the BG with a quarter wave phase shift region in the middle of the BG is shown in Fig. 7. The width of the transmission band can be made very small, thereby increasing the slope of the transmission window, which leads to increased sensitivity. Because of their higher transmission and narrower bandwidth, QWBGs have found widespread application in the field of optical communications especially in dense wavelength-division multiplexing (DWDM) and DFB laser technology. In this section, we discuss the application of these filters for AFM as a displacement sensor. A QWBG can be modeled as a Fabry–Perot resonator with the gratings serving as wavelength selective mirrors of identical reflection spectra separated by a quarter wave shifted region. The narrow transmission band appears in the middle of the stopband region when the length L of the quarter phase shift region satisfies the phase matching condition ($L = (n+1)(\lambda/4)$). The transmission bandwidth depends quantitatively on the coupling strength and length of the gratings mirror and waveguide loss. Using the same analysis as in the previous section, it is possible to have a bandwidth of 0.5Å and reflectivity of $R \geq 0.9$ which makes this sensor more sensitive than the standard BG by two orders of magnitude. Fig. 8 shows the output intensity variation as a function of the index change of the grating calculated using the results of numerical stress distribution for different cavity lengths. Large change in the output intensity is seen to occur for index change larger than 10^{-6}, indicating high sensitivity for large

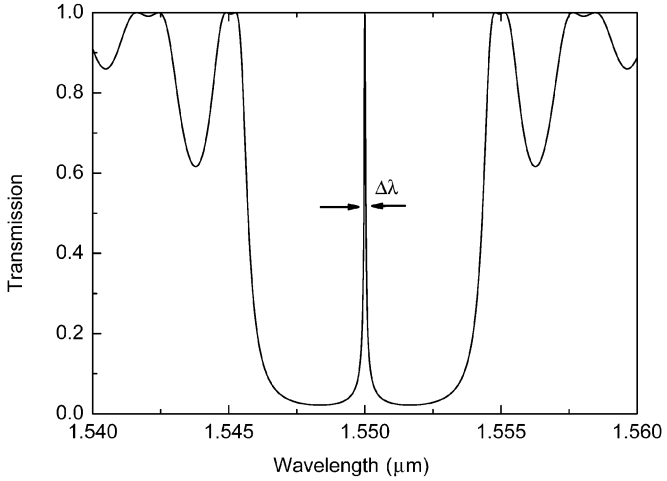

Fig. 7. Transmission spectrum of a BG with a quarter-wave phase shift. Note the sharp transmission peak at the center of the stopband.

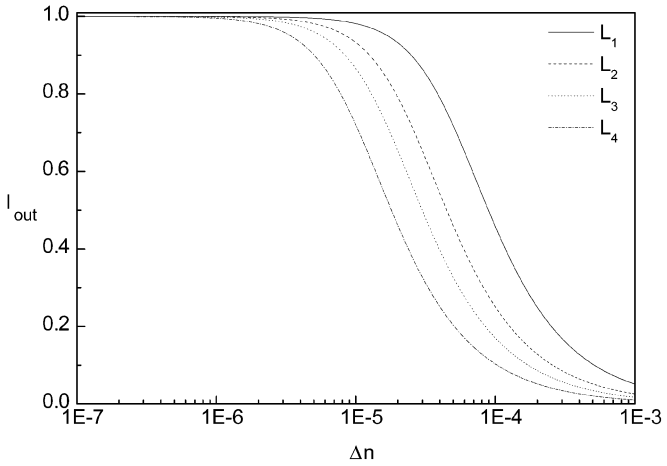

Fig. 8. Output intensity as a function of (stress induced) index change for four different lengths of quarter-wave phase shift region. Here, L_1, L_2, L_3, and L_4 are $101\times(\lambda/4)$, $201\times(\lambda/4)$, $301\times(\lambda/4)$, and $501\times(\lambda/4)$, respectively.

displacements. Interestingly enough, changes in output intensity saturates at large index changes indicating the loss of overlap between the laser wavelength and the reflection spectrum. For small displacements that create index changes below 1×10^{-6}, change in output intensity as high as 1×10^{-4} can be achieved with suitable choice of L_c. Higher values are limited by the length of the cantilever. Longer phase shifted regions provide more sensitivity for index change. In Fig. 9, we plot the normalized output intensity variation as a function of the cantilever displacement for two different cantilever lengths. It is clearly seen from the graph that for small displacements, the output intensity variation increases much more rapidly and is exponentially depended on the cantilever deflection.

VI. DESIGN OF EXPERIMENTAL SETUP

The design of experimental setup is very similar to fiber optic interferometer setup. A narrowband DFB laser with fiber output is used as the light source. The output of laser is split into two with a directional coupler one of which is used as reference to eliminate the intensity fluctuation of the laser. The other output is butt-coupled to the waveguide on the cantilever and reflected

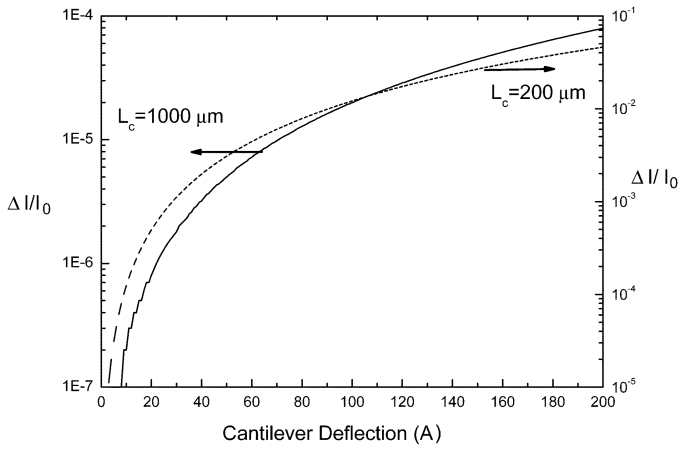

Fig. 9. Normalized output intensity change as a function of cantilever displacement for two different cantilever lengths.

light from BG is fed to a photodetector via the same directional coupler. Fluctuations of the laser wavelength causes intensity variations at the output. Balanced or lock-in amplification may be used to eliminate the random intensity variations.

VII. Sensitivity

The enhancement of force and displacement measurement sensitivity is of great interest since smaller deflections can be measured with greater accuracy. It should be mentioned that most previous integrated sensors provide less sensitivity than the external ones (i.e., Fabry–Perot interferometer). With this new design, the sensitivity can be enhanced by two orders of magnitude. Sensitivity can be defined as the variation of current on photodetector (PD) per unit displacement of cantilever. Current on PD is proportional to the intensity of the light falling on it, so that

$$\frac{\Delta i}{i} = \frac{\Delta I_{\text{out}}}{I_0} \tag{22}$$

from (12)

$$\frac{\Delta I_{\text{out}}}{I_0} = R4ln2\left(\frac{\Delta\lambda_c}{\Delta\lambda^2}\right)\exp\left[-4ln2\left(\frac{\lambda-\lambda_g}{\Delta\lambda}\right)^2\right]\frac{d\lambda}{dz}\Delta z. \tag{23}$$

We can write λ_g in terms of displacement or force on the cantilever

$$\lambda_g = 2\Lambda\left(n_0 + \frac{3C_lEt}{2l^2}z\right) = 2\Lambda\left(n_0 + \frac{6C_ll}{wt^2}F\right) \tag{24}$$

leading to

$$\frac{d\lambda_g}{dz} = \frac{3\Lambda C_lEt}{l^2} \tag{25}$$

or

$$\frac{d\lambda_g}{dF} = \frac{12\Lambda C_ll}{wt^2}. \tag{26}$$

As a result, we can define displacement sensitivity as

$$S_d = \frac{\Delta I_{\text{out}}}{I_0\Delta z} \tag{27}$$

which becomes

$$S_d = R\frac{12ln2\Lambda C_lEt}{l^2}\left(\frac{\Delta\lambda_c}{\Delta\lambda^2}\right)\exp\left[-4ln2\left(\frac{\lambda_L-\lambda_g}{\Delta\lambda}\right)^2\right] \tag{28}$$

and force sensitivity as

$$S_f = \frac{\Delta I_{\text{out}}}{I_0\Delta F} \tag{29}$$

which is given as

$$S_f = R\frac{48ln2\Lambda C_ll}{wt^2}\left(\frac{\Delta\lambda_c}{\Delta\lambda^2}\right)\exp\left[-4ln2\left(\frac{\lambda_L-\lambda_g}{\Delta\lambda}\right)^2\right]. \tag{30}$$

Photo-elastic displacement sensitivity is given in (27). This defines the changes in the output intensity per unit displacement of the cantilever. From (27), it is understood that displacement sensitivity depends on Young's Modulus and stress-optic coefficient. In order to achieve high sensitivity, cantilever material should be chosen such that it has high Young's modulus and stress-optic coefficient. GaAs is a very good material for displacement measurements. Force sensitivity can be defined as change in the output intensity per unit force applied on the cantilever. From (28), we can conclude that force sensitivity does not depend on the Young's modulus. This allows us to fabricate cantilevers from materials which have low Young's modulus but has large stress-optic constant such as some polymers. We also conclude from (27) and (28) that a short and thick cantilever is sensitive to displacement measurements whereas long and thin cantilevers are more sensitive to force detection. Fig. 9 shows normalized intensity change as a function of the cantilever displacement. Large changes in output intensity for large cantilever displacement of the order of few tens of angstroms are easily obtained for short cantilevers. Even for cantilever displacements of the order of a few angstroms, easily measurable changes in output intensity are possible. Additional improvement of sensitivity can be done by modifying the geometry of the cantilever. Maximizing the stress in the grating region will maximize the sensitivity. Such stress concentating regions on cantilevers have been studied by Bashir *et al.* [18]. This method can also be applied to the design presented here to increase the displacement sensitivity further.

VIII. Noise Considerations

The resolution of scanning force microscope is limited by the noise of the system. The minimum detectable distance (MDD) depends not only on the sensitivity but also on the noise of the microscope. Noise level of the system establishes the minimum detectable optical power on the photodetector necessary to obtain the cantilever displacement. For piezoresistive cantilevers, the fundamental noise is the Johnson noise in the piezoresistor [21]. For optical lever and interdigital detection techniques, the

fundamental noises are the shot noise of the photodetector and the noise due to thermal vibration of the cantilever. Displacement sensitivity is defined as the variation of the normalized output intensity per unit displacement of the tip. It can be written as

$$S_d = \frac{\Delta I}{I_0 \Delta z}. \tag{31}$$

The input intensity (power) I_0 depends on the light source and typically is of the order of few mWs. There are several noise sources in a displacement measuring cantilever system using integrated optical detection. The laser used to provide the signal is a source of noise. Not only the output intensity but also the phase and the frequency of a semiconductor laser may fluctuate in time. The cantilever displacement is measured directly from the optical intensity changes in the transmission spectrum of the ring resonator system; therefore, magnitudes of these fluctuations (noises) can be estimated. For a semiconductor laser, the intensity fluctuation noise is given as the relative intensity noise (RIN)

$$\mathrm{RIN} = \frac{(\delta P)^2}{P^2}. \tag{32}$$

DFB lasers with RIN of 160 dB/Hz are commercially available which is negligbly small. The laser intensity variation can be eliminated by introducing a reference photodetector with differential amplification and the output intensity can be normalized. For our design we choose a tunable laser source which provides high intensity and wavelength stability [23]. This laser provides 0.01-dB long-term intensity stability which translates into power variation of %0.1. Another important noise source is the random wavelength variations. For BG displacement sensors, the wavelength variation causes output intensity variation. In order to reduce this noise a laser which provides high wavelength stability can be used. There are commercially available tunable lasers with 0.1-pm wavelength stability which introduces intensity variations of %0.01 [23]. The intensity variation and wavelength variation can be reduced by using suitable light sources and lock-in amplification. On the other hand, laser pointing noise that needs to be considered for external optical detection methods, is totally eliminated in the BG system since laser is butt-coupled to the waveguide. An additional noise source is the thermal vibration of the cantilever. To analyze the thermal vibrational noise, the cantilever can be modeled as simple harmonic oscillator. At finite temperatures, the cantilever vibrates due to thermal excitation. The cantilever is subject to a random time-dependent Brownian motion around its equilibrium position. The thermal mechanical noise of the cantilever is estimated as [24]

$$\Delta z_{\mathrm{thermal}} = \sqrt{\frac{2k_b T B}{\pi Q k f_0}} \tag{33}$$

where k_b is the Boltzman constant, T is the temperature, B is the bandwidth, Q is the quality factor of the cantilever, k is the spring constant, and f_0 is the resonance frequency of the cantilever. To estimate the magnitude of the noise, a rectangular cantilever with length of 200-μm width of 50 μm and thickness of 5 μm is chosen. The resonance frequency is 50 kHz, the spring constant is 16 N/m and the bandwidth is about 1 kHz. The quality factor of the cantilever $Q = 100$ is chosen for analysis. At room temperature, the thermal vibrational noise is obtained as $\Delta z_{\mathrm{thermal}} = 0.0017$ Å which is very small. In the light of the data presented in Table I, it is clear that as the cantilever length increases, the stiffness will decrease and thermomechanical noise will increase and may in fact be dominant in cases of ultrasensitive force detection [8], [25]. There are two fundamental noises for detection electronics; shot noise and thermal noise. When the optical power is detected photons fall randomly on the photodetector and time average of the received power fluctuates due to the this randomness. The rms current due to shot noise is given by the well-known equation as

$$i_{\mathrm{shot}} = \sqrt{2eiB} \tag{34}$$

where e is the electron charge and B is the bandwidth. SNR can be written as

$$\mathrm{SNR} = \frac{i}{i_{\mathrm{shot}}} = \sqrt{\frac{i}{2eB}}. \tag{35}$$

SNR increases with the received power. For 100-μW optical power the shot noise current is $i_{\mathrm{shot}} = 6\ 10^{-10}$ A, SNR is 10^5 and shot noise limited MDD is 0.027 Å. Another noise source for photodetectors is the thermal noise in the detection electronics also known as Johnson noise. Random thermal motion of the electrons in a resistor produce a fluctuating current

$$i_{\mathrm{thermal}} = \sqrt{\frac{4kTB}{R}} \tag{36}$$

where k is the Boltzman constant, T is the temperature, and R is the resistance. For typical operational values, we obtain $i_{\mathrm{thermal}} = 4 \times 10^{-10}$ A which can easily be neglected. Finally, $1/f$ noise present in all electronic detection systems may become dominant if the cantilever is operated in the contact mode. The total noise is the sum of the all noise contributions. If the cantilever is operated in the noncontact mode to detect displacement and the received power is high enough, the dominant noise source is the shot noise. For 100-μW optical power, shot noise limited MDD is 0.027Å. SNR can also be increased by increasing the optical power.

Coupling light into and out of waveguides can be done in several different ways. Once aligned, optical fibers may be permanently fixed as is done for pigtailed lasers using standard packaging techniques. Tapering the waveguides at the input and output ports, to match the fiber mode size will increase the coupling efficiency, while V-grooves may be used to make the alignment process easier. On the other hand, if a proper semiconductor material such as GaAs is used to construct the cantilever, both a laser as the light source and a detector may eventually be fully integrated on the cantilever substrate. Operating point can be set at the steepest part of the reflection spectrum which can be determined by taking the derivative of the reflected power while scaning the laser from maximum transmisison to maximum reflection. As can be observed from Fig. 9, the change in the normalized output intensity is a nonlinear function of

cantilever deflection for very small deflections. In this regime, careful calibration of the nonlinear response will be necessary. However, as the deflection increases so that noncontact operation of the cantilever becomes possible, the normalized output intensity may be considered to be linear.

IX. Conclusion

In this paper, we introduced a novel high sensitive integrated optical displacement sensor for scanning probe microscopies. We analyzed the feasibility of the integrated optical sensor for micro cantilevers. The design of GaAs based cantilever with integrated BG has been described in detail. The concept based on the stress-optic effect was discussed. The principle experimental setup of this probe was described and theoretical investigation of the force and displacement sensitivity was presented. We find that integrated optical sensor is attractive because of its high sensitivity and simplicity. This design is a good alternative to piezoresistive cantilevers especially in electromagnetically active environments. This method has high potential for further improvement and has large application area such as lateral force microscopy. The advantage of this method is that it does not require any alignment and the setup is compact and it has high sensitivity.

Acknowledgment

The authors would like to thank Prof. A. Oral for an introductory discussion on cantilever designs.

References

[1] G. Binning, C. Quate, and C. Gerber, "Atomic force microscope," *Phys. Rev. Lett.*, vol. 56, pp. 930–933, 1986.
[2] Y. Martin, C. C. Williams, and H. K. Wickramasinghe, "Atomic force microscopeforce mapping and profiling on a sub 100-Å scale," *Appl. Phys. Lett.*, vol. 61, pp. 4723–4729, 1987.
[3] C. Mathew Mate, G. M. McClelland, R. Erlandsson, and S. Chiang, "Atomic-scale friction of tungsten tip on a graphite surface," *Phys. Rev. Lett.*, vol. 59, pp. 1942–1945, 1987.
[4] D. Rugar, H. J. Mamin, and P. Guethner, "Improved fiber-optic interferometer for atomic force microscopy," *Appl. Phys. Lett.*, vol. 55, pp. 2588–2590, 1989.
[5] G. Meyer and N. M. Amer, "Novel optical approach to atomic force microscopy," *Appl. Phys. Lett.*, vol. 53, pp. 1045–1047, 1988.
[6] S. R. Manalis, S. C. Minne, A. Atalar, and C. F. Quate, "Interdigital cantilever for atomic force microscopy," *Appl. Phys. Lett.*, vol. 69, pp. 3944–3946, 1996.
[7] M. Tortonese, H. Yamada, R. C. Barrett, and C. F. Quate, "Atomic force microscopy using a piezoresistive cantilever," in *Proc. IEEE Conf. Tranducers*, 1991, pp. 448–451.
[8] R. G. Knobel and A. N. Cleland, "Nanometer-scale displacement sensing using a single electron transistor," *Nature*, vol. 424, pp. 291–293, 2003.
[9] R. Linnemann, T. Gotszalk, I. W. Rangelow, and Oesterschulze, "Atomic force microscopy and lateral force microscopy using piezoresistive cantilevers," *J. Vac. Sci. Technol. B*, vol. 14, pp. 856–860, 1996.
[10] T. Gotszalk, P. Grabiec, and I. W. Rangelow, "Piezoresistive sensors for scanning probe microscopy," *Ultramicroscopy*, vol. 82, pp. 39–48, 1996.
[11] PCT, Int., Application No. PCT/TR03/05 (filed June 18, 2003).
[12] T. Storgaard-Larsen, S. Bouwstra, and O. Leistiko, "Opto-mechanical accelerometer based on strain sensing by a Bragg grating in a planar waveguide," *Sens. Actuators A*, vol. 52, pp. 25–32, 1996.
[13] K. Okamoto, *Fundamentals of Optical Waveguide*. New York: Academic, 1992.
[14] S. M. Melle, K. Liu, and M. Measures, "A passive wavelenght demodulation system for guided-wave Bragg grating sensors," *IEEE Photon. Technol. Lett.*, vol. 4, no. 3, pp. 516–520, Mar. 1992.
[15] Y. Youlong, T. Hwayaw, C. Wenghong, and M. S. Demokan, "Opto-mechanical accelerometer based on strain sensing by a Bragg grating in a planar waveguide," *Opt. Lett.*, vol. 25, pp. 1141–1141, 2000.
[16] A. Yariv and H. V. Winsor, *Opt. Lett.*, vol. 5, pp. 87–89, 1980.
[17] L. A. Ferreira, E. V. Diatzikis, P. J. Moreira, J. L. Santos, and F. Farahi, "Application of multimode laser diodes in the interrogation of fiber Bragg grating sensors," *Opt. Fiber Technol.*, vol. 6, pp. 365–387, 2000.
[18] R. Bashir, A. Gupta, G. W. Neudeck, M. McElfresh, and R. Gones, "On the design of piezoresistive silicon cantilever with stress concentration region for scanning probe microscopy application," *J. Micromech. Microeng.*, vol. 10, pp. 483–491, 2000.
[19] W. Streifer, D. R. Scifres, and R. D. Burham, "Coupling coefficients for distributed feedback single- and double-heterostructure diode lasers," *IEEE Quantum Electron.*, vol. QE-11, no. 6, pp. 867–873, Jun. 1975.
[20] H. A. Haus and R. V. Schmidt, *IEEE Trans. Sonic Ultrason.*, vol. SU-24, no. 1, pp. 94–94, Jan. 1977.
[21] O. Hansen and A. Boisen, "Noise in the piezoresistive atomic force microscopy," *Nanotechnology*, vol. 10, pp. 51–60, 1999.
[22] 79 800D DFB Source Module, ILX Lightwave Corporation.
[23] Tunable laser Source TLS 8800 Series, ILX Lightwave Corporation.
[24] S. Rast, C. Wattinger, U. Gysin, and E. Meyer, "The noise of cantilever," *Nanotechology*, vol. 11, pp. 169–172, 2000.
[25] J. A. Harley and T. W. Kenny, "High-sensitivity piezoresistive cantilevers under 1000 Å thick," *Appl. Phys. Lett*, vol. 75, pp. 289–291, 1999.

Coskun Kocabas, photograph and biography not available at the time of publication.

Atilla Aydinli (M'99) was born in Canakkale, Turkey in 1953. He graduated from the Enginering Physics Department, Hacettepe University, Ankara, Turkey, in 1975 and received the M.S. and Ph.D. degrees from the University of Virginia, Charlottesville, in 1981.

He was an Assistant and Associate Professor with the Engineering Physics Department, Hacettepe University, until 1991. He was appointed to Professor at Bilkent University, Ankara, in 1992. He was a Visiting Professor at University of Padua, Padua, Italy, from 1986 to 1987, where he worked on strain measurements of MBE grown InGaAs using RBS and channeling. From 1989 to 1990, he worked on laser ablation and deposition of II–VI semiconductors at The University of Toledo, Toledo, OH, and, from 1997 to 1998, he worked on GaAs-based integrated optical devices at the University of Santa Barbara, Santa Barbara, CA. His current research interests include optical spectroscopy of nanocrystals, integrated optical devices, and nanosensing with IO devices.